ON THE NONLINEAR DYNAMICS APPROACH OF MODELING THE BIFURCATION FOR TRANSONIC LIMIT CYCLE FLUTTER

H. Matsushita[*], T. Miyata[*], L. E. Christiansen[**], T. Lehn-Schiøler[**], and E. Mosekilde[***]
[*]Fukui University, Fukui, Japan
[**]Technical University of Denmark, Lyngby, Denmark

Keywords: *Transonic flutter, limit cycle oscillation, bifurcation, mathematical model*

Abstract

This paper reports the improvement of the two-degrees-of-freedom, finite dimensional, nonlinear math model, which has been proposed and developed by the authors to explain every feature of the transonic flutter data of the wind tunnel tests conducted at National Aerospace Laboratory in Japan for a high aspect ratio wing. It enables to explain the nonlinear features of the transonic flutter such as the subcritical Hopf bifurcation of a limit cycle oscillation (LCO), a saddle-node bifurcation, and an unstable limit cycle. By making use of the continuation method for analyzing the bifurcation nature of the math model, quantitative matching is obtained for the LCO amplitude between the math model and the test results. The wing deflections which are defining the bifurcation and were previously obtained by numerical integration of the acceleration data are now confirmed by the direct measurement of the deflection using newly developed laser deflection measuring device.

1 Introduction

In transonic regions flutter often takes the form of a limit cycle oscillation (LCO) caused by the nonlinearity of the transonic aerodynamics due to a shock wave moving on the wing surface coupled with the flow separation [1]-[3]. Recent tests in the transonic wind tunnel at National Aerospace Laboratory in Japan for a high aspect ratio wing have revealed a lot of bifurcation phenomena. Every flutter occurred suddenly as a subcritical Hopf bifurcation, jumping up to large amplitude LCO, while decreasing a dynamic pressure kept LCO continued until a saddle-node bifurcation point, where the wing stopped to oscillate. In such a way transonic flutter has a hysteresis in LCO occurrence. In between this range, a stability boundary (unstable limit cycle) was identified which separates the regions into two groups: one going up to LCO and the other going down to equilibrium [4]-[6].

The authors have developed, by the nonlinear dynamics approach, a two-degrees-of-freedom (2-DOF) nonlinear mathematical model, which has fourth order nonlinear terms in the diagonal components of the aerodynamics damping [7]. The model can explain qualitatively the fundamental bifurcation phenomena listed above. It also can predict a lot of important noise effects on the subcritical Hopf bifurcation such as noisy precursors, a coherent resonance, and even a stochastic resonance [8].

The model has two sets of free parameters, which are to be determined to fit the test data. With parameters chosen so far, the model cannot attain quantitative matching with the test results; mathematically predicted amplitude of LCO is rather smaller than the amplitude analyzed by the test data. Further examination to what extent this model can be improved by optimizing the parameters in the model, therefore, is necessary. In the following chapters, the authors investigate this problems in two ways: in one way, the bifurcation diagram that was obtained by numerically integrating the accelerometers output is examined by a set of deflection data, which is newly obtained by direct

measurement of the deflection using a laser optical measurement device. The other approach is taken to conduct parametric study of changing the parameters in the math model making use of a continuation method for analysis of the bifurcation diagram.

2 Experimental Observation of Bifurcation in Transonic Flutter and Its Nonlinear Math Model

2.1 Experimental Observation

Figure 1 shows a wind tunnel model of a high aspect ratio wing. It has a leading edge and a trailing edge control surfaces. They are used for active flutter control research [9]. Basically the wing has a supercritical section except at an inflated middle part where the wing section is symmetrical and two sets of electric motors are installed. For LCO investigation in the wind tunnel tests, a leading edge control surface is used as a source of excitation and wing response is measured by four accelerometers and seven sets of torsion and bending strain gages, which are fixed at an aluminum spar of the wing.

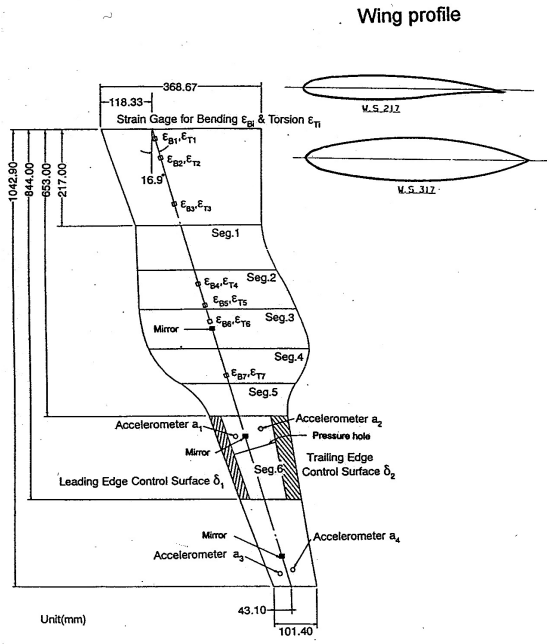

Fig. 1 High aspect ratio wing model

In the series of wind tunnel experiments at the transonic wind tunnel of the National Aerospace Laboratory in Japan, it was turned out that this wing behaves a typical transonic flutter. The wing has transonic dip phenomena and every flutter has the form of LCO. In each flutter, when the tunnel pressure is increased as shown at the bottom chart in Fig. 2 as a typical case of Mach 0.8, the wing jumps up to LCO at a specified (nominal) dynamic pressure as shown at the top chart in the figure. (Since this figure shows the active flutter test result [9], the LCO flutter is stopped right after its occurrence by activating a trailing edge control surface as shown at the middle chart.) Successive investi-

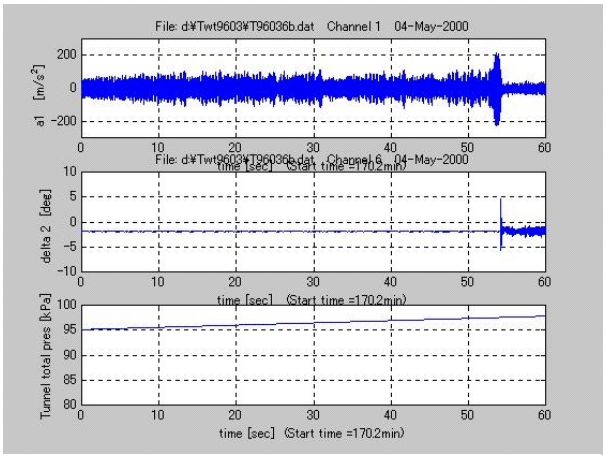

Fig. 2 Time history of nominal flutter occurrence during the increase of the wind tunnel pressure.

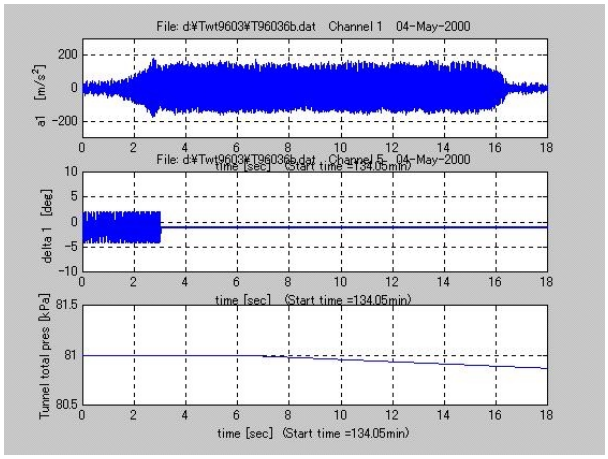

Fig. 3 Quasi-steady decrease of the dynamic pressure at the saddle-node bifurcation

gation cleared that, even at lower dynamic pressure than the nominal pressure stated above, the wing can be brought into LCO state if it's excited above a certain energy level. Once LCO state is attained, it is kept continuing even after removing the excitation. LCO thus attained is stabilized again if the tunnel pressure is further decreased. These phenomena are presented in Fig. 3 where the LCO is established by a leading edge excitation as shown at the middle chart in this case, and continues to oscillate even after removing the excitation. Then LCO continues to oscillate during the quasi-steady decrease of the wind tunnel pressure until it ceases to rest at a certain value of the pressure. That point corresponds to a saddle-node bifurcation.

Figure 4 summarizes these phenomena found in the tests as a bifurcation diagram where the LCO amplitude is depicted against the dynamic pressure. In this figure the stability boundary, or unstable limit cycle expressed by the crosses, has a significant deviation and the stable region under the boundary is rather narrow. Disturbances around the wing such as turbulence in the wind tunnel flow, the flow separation occurred at the wing surface, etc., may decrease the stable region in the experimentally obtained diagram. This point will be discussed further again in Chapter 3.

In the previous tests wing surface deflections were not measured directly but the accelerometers attached to the wing spar measured the acceleration. The LCO amplitude was obtained numerically integrating the acceleration data. In the latest test, a laser optical deflection device of an ultra long rage was developed and introduced to the test. Validation of the integrated deflection will be discussed in chapter 4.

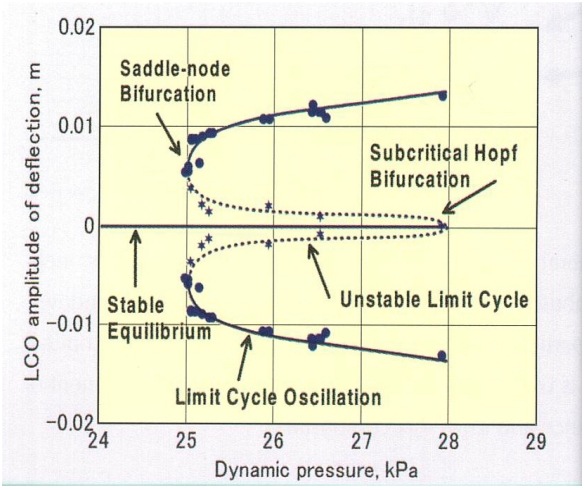

Fig. 4 Bifurcation diagram obtained by the wind tunnel tests

2.2 Nonlinear Mathematical Model

The basic principle of modeling is to construct a model that is as simpler as possible and still have a physical meaning and can explain the wind tunnel test observation. As a simplest model, the first author *et al*. have developed a nonlinear mathematical model in the form of a 2-DOF, finite state nonlinear differential equation [7]. Introducing the fourth order nonlinearity in q_i, i=1,2 to the generalized aerodynamic damping terms, they have obtained the following sixth order nonlinear differential equation,

$$\dot{x} = (A + \Delta A_{NL})x; \quad x = [q,\ \dot{q},\ z]^T \in R^6 \qquad (1)$$

where q is the generalized coordinates and z is the augmented variable expressing the unsteady aerodynamic delay. The matrix A is a linear part of the system matrix and is an ordinary matrix for flutter analysis. It takes a form as,

$$A=\{a_{ij}\}=\begin{bmatrix} 0 & I & 0 \\ -(M-A_0)^{-1}(K-A_2) & -(M-A_0)^{-1}(C-A_1) & -(M-A_0)^{-1} \\ B_a & 0 & -\Lambda \end{bmatrix} \in R^{6\times 6} \qquad (2)$$

In this equation M, C, and K are mass, structural damping, and stiffness matrices, respectively, used in the following fundamental aeroelastic equation of a flexible wing.

$$M\ddot{q} + C\dot{q} + Kq = f_a \qquad (3)$$

The aerodynamic term f_a in right hand side is approximated by the finite state form:

$$\begin{aligned} f_a &= A_2\ddot{q} + A_1\dot{q} + A_0 q + z \\ z &= \Lambda z + B_0 q \end{aligned} \qquad (4)$$

where $\Lambda = diag(-\lambda,\cdots,-\lambda)$.

The matrix ΔA_{NL} in eq. (1) represents a nonlinear terms and has the following form.

$$\Delta A_{NL}=\begin{bmatrix}0 & 0 & 0\\ 0 & (M-A_0)^{-1}\Delta A_{1NL} & 0\\ 0 & 0 & 0\end{bmatrix}\in R^{6\times 6} \tag{5}$$

where the diagonal components of the aerodynamic damping part $(M-A_0)^{-1}\Delta A_{1NL}$ has the fourth order nonlinear terms such as

$$\Delta A_{1NL}=\begin{bmatrix}(\beta_1 q_1^{\,2}+\gamma_1 q_1^{\,4})a_{11a} & 0\\ 0 & (\beta_2 q_2^{\,2}+\gamma_2 q_2^{\,4})a_{22a}\end{bmatrix} \tag{6}$$

where a_{11a} and a_{22a} are the aerodynamic damping coefficients for torsion and bending deflection, respectively. The parameters β's and γ's are free parameters to be determined to fit the wind tunnel test data. When the parameters β's and γ's are set to be zero, the equation (1) is reduced to an ordinary linear flutter equation.

In order to make comparison with the test results, an output equation that relates the state variables in Eq. (1) with the output variables measured in the wind tunnel tests is necessary. Since two sets of measured and derived variables, acceleration a_1, a_2, velocity v_1, v_2 and deflection d_1, d_2 at two accelerometer positions on the wing are enough for comparison, the output equation will take the form

$$y=Cx;\ y=[a_1,a_2,v_1,v_2,d_1,d_2]^T\in R^6 \tag{7}$$

A set of equations (1) and (7) comprises the nonlinear 2-DOF math model for transonic flutter.

Nonlinear simulation of solving the equations (1) and (7) was conducted by making use of MATLAB/Simulink software. The coefficients in the math model was set as $\beta_1=\beta_2=-0.5$, $\gamma_1=\gamma_2=0.2$ since this set of values are reference ones for a typical 1-DOF nonlinear differential equation, which gives an LCO solution of a subcritical Hopf bifurcation type. For each dynamic pressure, simulation was conducted by changing equal initial conditions for x_1 (= q_1) and x_2 (= q_2) with the other states equal to zero. In Fig. 5 the simulation results in term of the deflection at the accelerometer #1 are displayed with circles and crosses. With this method of simulation it was difficult to get the points further near to the saddle-node bifurcation as shown in the figure.

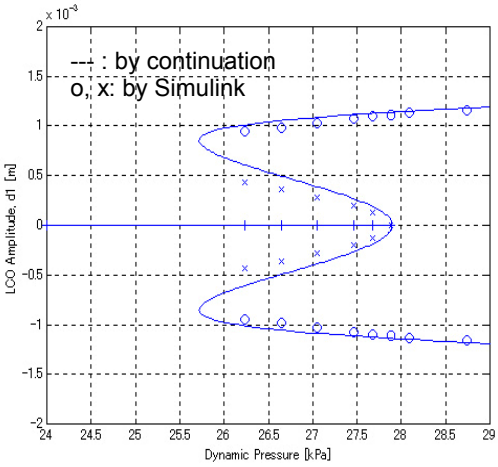

Fig. 5 Bifurcation diagram of 2-DOF nonlinear equation (1)

The Danish authors have applied the continuation method to the math model (1) modifying a computer program package of the method [10]. The package features a fourth order Runge-Kutta integrator with fixed size which is capable of making analysis of limit cycles using Poincaré sections as the control parameter (dynamic pressure in the present case) is continuously changing. The continuation method can thus trace continuously the Poincaré section, even through the unstable limit cycle branch, once at the initial stage LCO amplitude has been captured. They could obtain the smooth curve in the bifurcation diagram as shown as a solid line in Fig. 5. The continuation and the Simulink results are almost identical except at the unstable limit cycle branch and the saddle-node bifurcation area where some difference can be noticed. The former difference will be discussed in the next chapter. Figure 5 has a good correspondence with the test results in Fig. 4 at least qualitatively in that it explains every feature of nonlinear phenomena such as the subcritical Hopf bifurcation, a saddle-node bifurcation, and an unstable limit cycle. However Fig. 5 still has a large difference from Fig. 4 in amplitude of LCO. The math model has one-order smaller amplitude than the experimental results.

3 Parameter Optimization by Continuation Method

Christiansen and Lehn-Schiøler studied the effect of the parameters β's and γ's on the bifurcation diagram [10]. Particularly they got the amplitude and the velocity map at the saddle-node bifurcation for each bending parameters (β_1, γ_1) with torsion parameters (β_2, γ_2) neglected. Decreasing β_1 gives larger amplitude near the saddle-node and also moves it to a higher velocity. γ_1 can be used to adjust the amplitude.

Based on this study, parametric study has been executed to explore the proper values for the parameters in order that the analytical bifurcation diagram comes closer to the experimental one. The constraint of exploring is the condition that the bifurcation diagram should keep the distance of 10 % between the subcritical point and a saddle-node point, which corresponds to the experimental results. We started to search the optimal direction of the set of parameters β's and γ's to change in order to increase the LCO amplitude. Applying the continuation method to Eq. (1) with the two parameters doubled and halved, we can get the sensitivity chart as shown in Figure 6. The figure shows that as γ is reduced, the amplitude of LCO increases but the saddle-node bifurcation point greatly decreases, and as β is reduced in its absolute value, the saddle-node point increases a little, keeping the amplitude of LCO almost unchanged. Consequently the right direction we have to take may be upper left direction.

Making a lots of efforts to search an optimum combination of parameters, we have reached the values of β = -6.5e-3 and γ= 2.5e-5. It is worth notifying that the parameters thus obtained are surprisingly small, which means that a small nonlinearity is enough to put a wing into LCO state.

Resulting bifurcation diagram is shown as a solid line in Fig. 7. In the figure experimental data are also plotted. The correspondence of the LCO between the math model and the experiment is quite good; the amplitude of LCO is

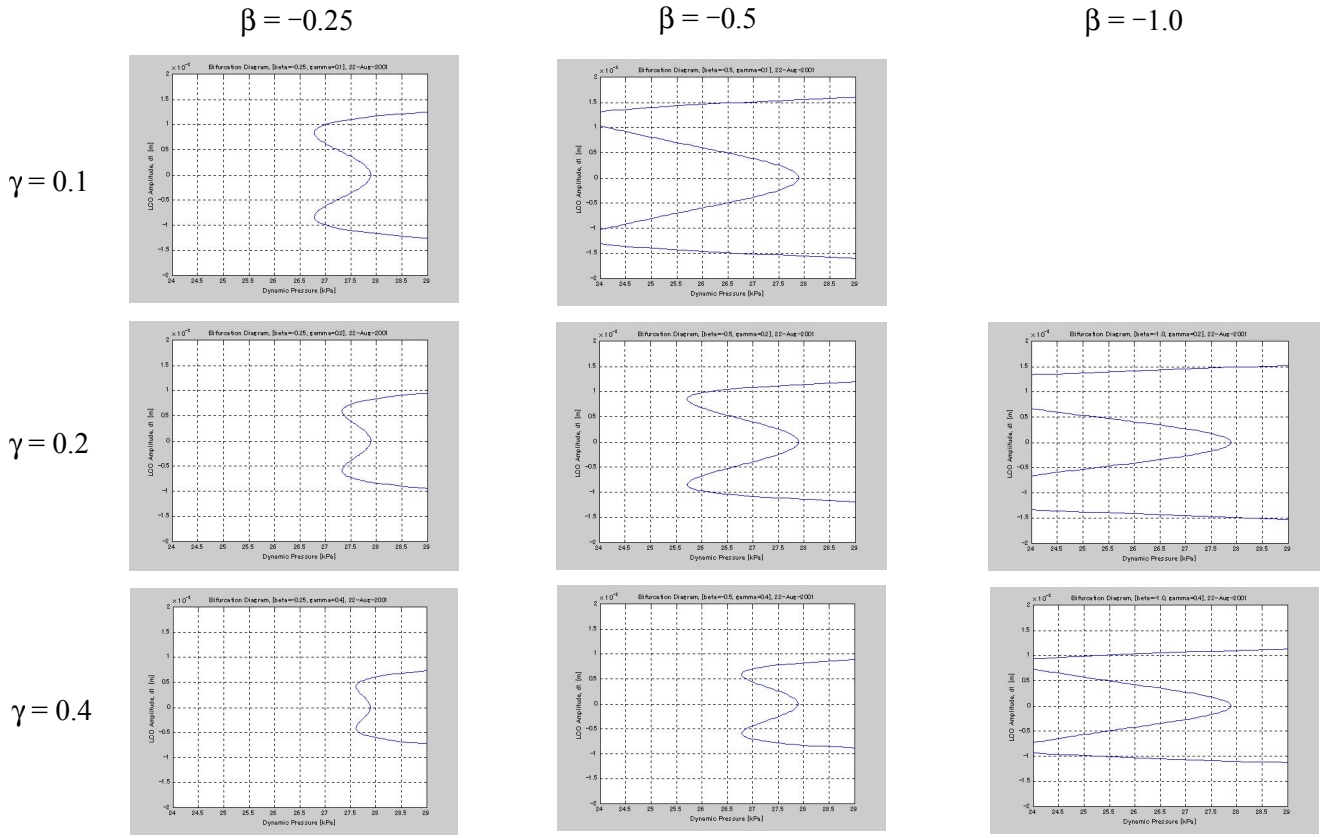

Fig. 6 Parameter sensitivity for increasing the amplitude of LCO

almost identical and the position of the saddle-node bifurcation is exactly the same. There still remains a difference in unstable limit cycle; the mathematical model has a wide stable area under the unstable limit cycle, while the experimental data shows a limited region of stability. As stated earlier, the main reason of this discrepancy may exist in the noise effects. In real situation, even at the stable region disturbance may energize the wing to jump up to unstable region and push the wing to LCO state.

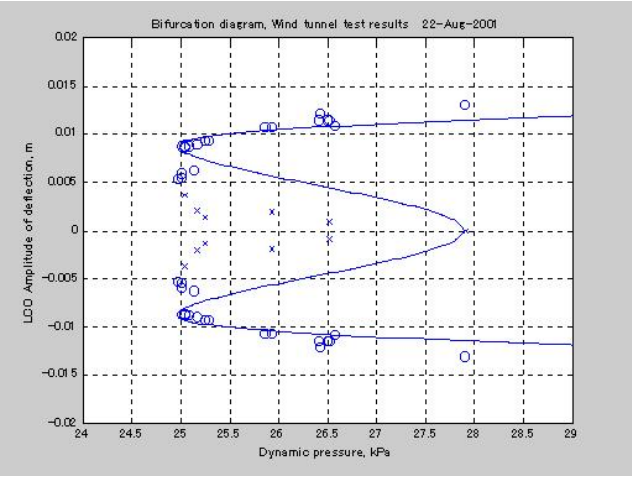

Fig. 7 Bifurcation diagram of the math model with optimized parameters and the experimental results.

4 Examination of the Deflection Data

Previously a wing deflection was not directly measured, but it was obtained by numerically integrating the acceleration data. Since integrated data may have a numerical error, a laser deflection measurement device has been developed to directly measure a wing surface deflection. The wind tunnel test was recently conducted to measure the wing deflection and acceleration at the same time.

Figure 8 is a typical result of measurement at the first flutter case in the recent test. The figure shows, from top to bottom, original voltage outputs from #1 and #2 accelerometers and #1 and #2 laser deflection devices. As can be seen, accelerometer outputs contain higher harmonics

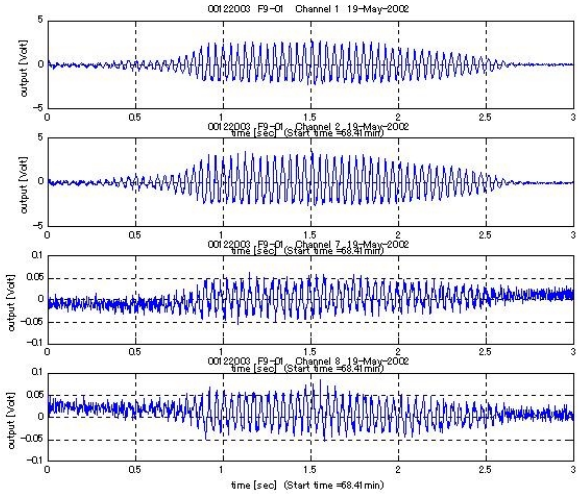

Fig. 8 Wind tunnel test data of accelerometers and laser deflection devices at flutter (M=0.8).

components, while laser deflection outputs are small and contaminated by the noise.

The accelerometer outputs are integrated by the following procedure; after subtracting the mean value, acceleration signal is integrated once to get the velocity. Then low frequency components contained in the velocity such as the bias and trend are filtered out applying a high pass Butterworth filter of 7.5 Hz cut-off frequency. Integration is applied once more and the deflection is obtained. Attenuation ratio introduced by these process is 97% which was obtained using the test function of $360\sin(2\pi ft)$ [m/s^2], where the frequency was taken nearly equal to flutter frequency, $f = 23.9$Hz.

Newly developed laser deflection measurement device has a very long range. A set of mirrors is installed to make separation between the laser emission point and the detection point larger so that a ultra-long range from 250mm to 750mm of the commercial device is further enlarged. It has the deflection range from 437mm to 1316mm and can measure the deflection of the wing from outside the wind tunnel. The wing is placed at the center of the test section of 2m×2m square. Two sets of the devices were developed and attached outside of the wind tunnel sidewall. They measured two points of accelerometers at the wing surface through the holes of the perforated wall. Problem exists in that the measuring range of the wing deflection

is rather small compared with the wide full range of the device. As will be seen in the next Figure 9, the wing deflection is at most 50mm p-p against 877mm full range, i. e., measurement uses only 5.7% of full range.

Figure 9 shows a result of data processing. In the figure first two channels are deflections d_{1i} and d_{2i} obtained by integrating twice a_1 and a_2 acceleration, respectively; while the next two channels are directly measured deflections, d_{1d} and d_{2d}. Actually a low pass filter of 30Hz cut-off frequency is applied in order to filter out the noise components. It can be seen that there is a difference between two sets of deflections; the integrated deflection is 72% of the direct measurement.

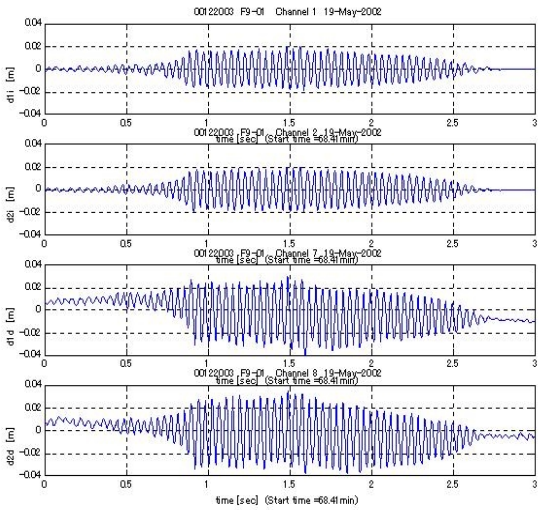

Fig. 9 Comparison of a wing surface deflection between integrating accelerometer signal and direct measuring by laser deflection device.

Although the direct measurement of the wing deflection produces a small level of signal containing a noise and the differences between two sets of deflection are not small, the integrated deflection used so far for defining the bifurcation diagram is checked out for the first time by direct measurement and it can be concluded that the integrated deflection, and the integrated velocity as well, has a reasonable value and can be used to define a phase diagram and bifurcation but with consideration of 20 to 30 % amplification in amplitude.

5 Conclusions

This paper reports the present status of improving the simple 2-DOF nonlinear mathematical model of a transonic limit cycle flutter. The model has an ordinary flutter equation of the first (bending) mode and the second (torsion) mode coupling type in a state space representation as a linear part, and has a fourth order nonlinearity in aerodynamic damping parts. By making use of the continuation method of continuously tracking the bifurcation diagram of the math model, parameter optimization is tried and quantitative matching is obtained for the LCO amplitude between the math model and the test results. Resulting model enables to explain quantitatively an LCO amplitude, a subcritical Hopf bifurcation, and a saddle-node bifurcation, which were observed in the transonic wind tunnel test at National Aerospace Laboratory in Japan for a high aspect ratio wing. There still has discrepancy for the unstable limit cycle with the wind tunnel tests, which suggests the limitation of this type of a model.

Acknowledgement

Authors would like to acknowledge Mr. Saitoh, Mr. Hashidate, and the other members of the group at NAL for executing a series of wind tunnel testing. They also appreciate Dr. Gránásy, GE Hungary Ltd. for introducing us a nonlinear dynamics view point to interpret our experimental observation.

References

[1] Cunningham, A. M., Jr. Practical problem: airplanes. Chapter 3, *Unsteady transonic aerodynamics*, Nixon, D., ed., Progress in Astronautics and Aeronautics, 120, AIAA, pp. 75-132, 1989.

[2] Dowell, E. H. Nonlinear Aeroelasticity. *Flight-Vehicle Materials, Structures and Dynamics*, 5, Part Ⅱ, Chapter 4, ASME, pp. 213 – 239, 1993.

[3] Schewe, G. and Deyhle, H. Experiments on transonic flutter of a two-dimensional supercritical wing with emphasis on the non-linear effects. *Proceedings of the Royal Aeronautical Society Conference on "UNSTEADY AERODYNAMICS"*, 1996.

[4] Gránásy, P., Matsushita, H., and Saitoh, K. Nonlinear analysis of transonic flutter. *Proceedings of the 10th*

International Sessions in Aircraft Symposium, JSASS, PP. 66-69, 1996.

[5] Gránásy, P., Matsushita, H., and Saitoh, K. Nonlinear aeroelastic phenomena at transonic region. *Proceedings of CEAS International Forum on Aeroelasticity and Structural Dynamics 1997*, Vol. Ⅲ, Rome, pp. 379-385, 1997.

[6] Matsushita, H., Saitoh, K., and Gránásy, P. Nonlinear characteristics of transonic flutter of a high aspect ratio wing. *Proceedings of 21st ICAS*, Melbourne, pp. 1-7, 1998.

[7] Matsushita, H., Saitoh, K., and Gránásy P. Two degrees-of-freedom nonlinear math model with fourth order nonlinear aerodynamics for transonic limit cycle flutter. *CEAS/AIAA/ICASE/NASA LaRC International Forum on Aeroelasticity and Structural Dynamics 1999*, Williamsburg, US, June 1999.

[8] Christiansen, L. E., Lehn-Schiøler, T., Mosekilde, E., Gránásy, and Matsushita, H. Nonlinear characteristics of randomly excited transonic flutter. *Mathematics and Computers in Simulation on Control of Oscillations and Chaos*, Vol. 58, pp. 385 – 405, 2002.

[9] Saitoh, K. Baldelli, D. H. Matsushita, H., and Hashidate, M. Robust controller design and its experimental validation for active transonic flutter suppression. *Proceedings of CEAS International Forum on Aeroelasticity and Structural Dynamics 1997*, Vol. Ⅱ, Rome, 1997, pp. 393-399.

[10] Christiansen, L. E. and Lehn-Schiøler, T. Stochastic modeling of transonic flutter. Department of Physics, The Technical University of Denmark, Denmark, 2000.